Review on Ocean Heat Content and Ocean Warming

Lei Huang

Abstract

Since the mid-20th century, there is substantial increase in the average measured temperature of the Earth's near-surface air and oceans, which is now known as "global warming". Global mean surface temperature increased 0.74 ± 0.18 °C during the 100 years ending in 2005. The Intergovernmental Panel on Climate Change (IPCC) concludes that most of the increase since the mid-twentieth century is "very likely" due to the increase in anthropogenic greenhouse gas concentrations. Natural phenomena such as solar variation combined with volcanoes probably had a small warming effect from pre-industrial times to 1950 and a small cooling effect from 1950 onward. Climate model projections summarized by the IPCC indicate that average global surface temperature will likely rise a further 1.1 to 6.4 °C during the twenty-first century. This range of values results from the use of differing scenarios of future greenhouse gas emissions as well as models with different climate sensitivity. Although most studies focus on the period up to 2100, warming and sea level rise are expected to continue for more than a thousand years even if greenhouse gas levels are stabilized. The delay in reaching equilibrium is a result of the large heat capacity of the oceans. In this review, the temporal and spatial variability of the heat content in the world ocean are estimated, and temperature changes in different layers of the ocean are compared with model results. Besides, linear trends in salinity for the world ocean from 1955 to 1998 are calculated and analyzed.

1. Introduction

Oceans cover approximately 71% of the Earth's surface and have great impact on the biosphere. The evaporation of these oceans is how we get most of our rainfall, and their temperature determines our climate and wind pattern. The Intergovernmental Panel on Climate Change (IPCC) (1995), the World Climate Research Program (WCRP) (1995) and the U.S. National Research Council (NRC) (1999) have identified the role of oceans as being critical to understanding the variability of Earth's climate system. Physically we expect this to be so because of the high density and specific heat of seawater. Oceans also have the thermal inertia and heat capacity to help maintain and ameliorate climate variability.

Studies using instrumental data to evaluate a warming trend of Earth's climate system due to increasing concentrations of greenhouse gases (GHGs) have focused on surface air temperature and sea surface temperature (IPCC 1995). These variables have shown an average warming of approximately 0.6°C at Earth's surface during the past 100 years. Recent comparisons (Mann et al. 1998; Mann 1999; Briffa et al. 1995) with paleoclimatic proxy data indicate that the observed increase in surface temperature during the past century is unprecedented during the past 1000 years. The results of these studies, along with similar results found using general circulation model (GCM) and energy balance model (Tett et al. 1999; Crowley 2000; Delworth et al. 2000; Stott et al. 2000), which include forcing by the observed time-dependent increase in GHGs and sulfate aerosols, as well as changes in solar irradiance and volcanic aerosols, provide evidence that the warming of Earth's surface during the past few decades is of anthropogenic origin. Despite the agreement between models and observations, it is conceivable that some of

the surface warming might be compensated by a cooling of other parts in Earth's climate system. Conversely, additional warming may be occurring in other parts of the climate system, such as the recently observed warming of the world ocean (Levitus et al. 2000).

In this review, we first looked at the interannual-to-decadal variability of the heat content (mean temperature) of the world ocean from the surface through 3000 m depth for the period 1948-1998 (Levitus et al. 2000), then we compared the temporal variability of the heat content of the world ocean, of the global atmosphere, and of components of Earth's cryosphere during the latter half of the 20th century (Levitus et al. 2001). The results of two different models forced by observed and estimated concentrations of greenhouse gases and the direct effect of sulfate aerosols on the atmosphere are compared with observations (Barnett et al. 2001; Levitus et al. 2001). Interannual variability in upper ocean heat content is studied using satellite altimetric height combined with in situ temperature profiles (Willis et al. 2004). At last, salinity changes during the period 1955-1998 for the world ocean are estimated to study the large-scale trends in salinity over this period (Boyer et al. 2005).

2. Temporal Variability of Upper Ocean Heat Content

Figure 1 shows the variability of yearly heat content anomalies in the upper 300 m for 1948 to 1998 for individual ocean basins defined using the Equator as a boundary. The anomaly fields for the Atlantic and Indian oceans, for both the entire basins and Northern and Southern Hemisphere basins of each ocean, show a positive correlation. In each basin before the mid-1970s, temperatures were relatively cool, whereas after the mid-1970s these oceans are in a warm state. The year of largest yearly mean

temperature and heat content for the North Atlantic is 1998.

Both Pacific Ocean basins exhibit quasi-bidecadal changes in upper ocean heat content, with the two basins positively correlated. During 1997 the Pacific achieved its maximum heat content. A decadal-scale oscillation in North Pacific sea surface temperature (Pacific Decadal Oscillation) has been identified (Nitta et al. 1989; Trenberth 1991), but it is not clear if the variability we observe in Pacific Ocean heat content is correlated with this phenomenon or whether there are additional phenomena that contribute to the observed heat content variability.

Figure 2 shows the heat content for 5-year running composites by individual basins integrated through 3000-m depth. The distributions are presented through 3000-m depth for consistency. There is a consistent warming signal in each ocean basin, although the signals are not monotonic. The signals between the Northern and Southern Hemisphere basins of the Pacific and Indian oceans are positively correlated, suggesting the same basin-scale forcings. The temporal variability of the South Atlantic differs significantly from the North Atlantic, which is due to the deep convective processes that occur in the North Atlantic. Before the 1970s, heat content was generally negative. The Pacific and Atlantic oceans have been warming since the 1950s, and the Indian Ocean has warmed since the 1960s. The delayed warming of the Indian Ocean with respect to the other two oceans may be due to the sparsity of data in the Indian Ocean before 1960. The range of heat content for this series is on the order of 20×10^{22} J for the world ocean.
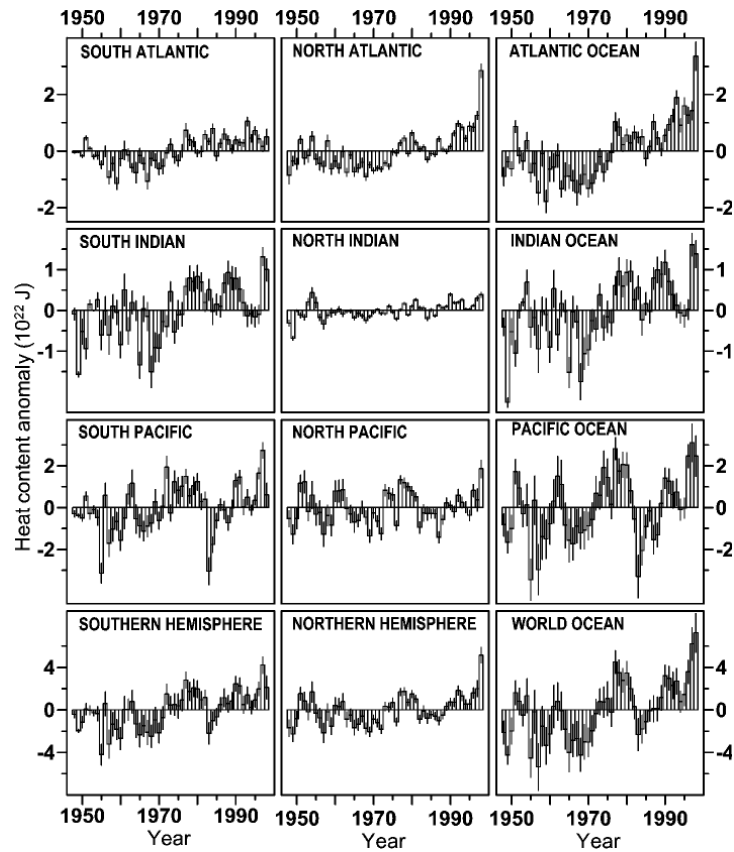
Fig. 1. Time series for the period 1948-1998 of ocean heat content (10^{22} J) in the upper 300 m for the Atlantic, Indian, Pacific, and world oceans.
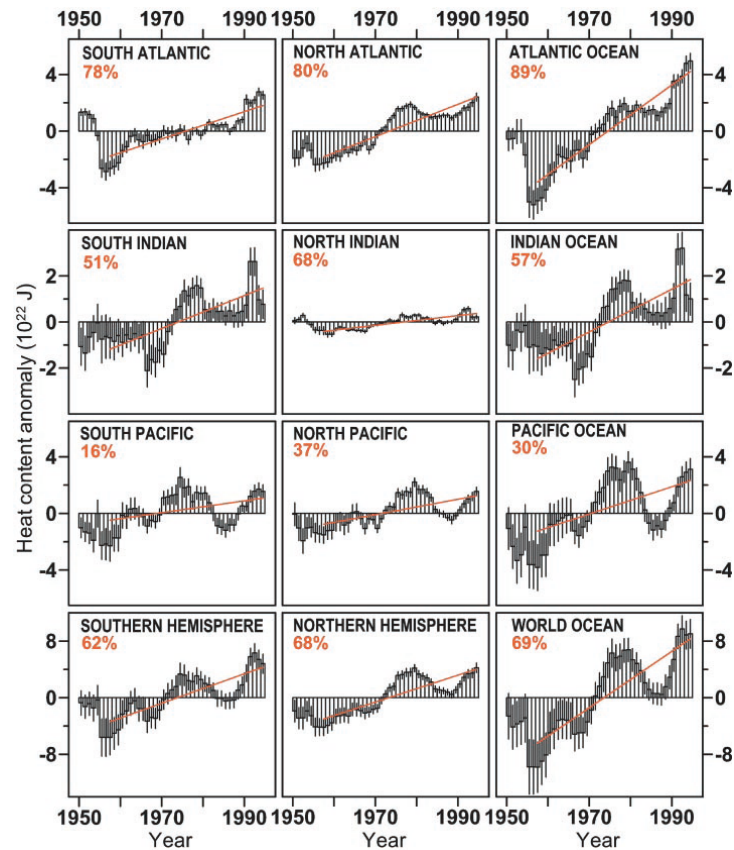
Fig. 2. Time series of 5-year running composites of heat content (10^{22} J) in the upper 3000 m for each major ocean basin. The linear trend is estimated for each time series for the period 1955-1996, which corresponds to the period of best data coverage. The trend is plotted as a red line. The percent variance accounted for by this trend is given in the upper left corner of each panel.

3. GCM Model simulation results compared with observations

Figure 3 shows the estimated temporal variability of global ocean and atmospheric heat content, based on instrumental data for the 1955-1996 period. The atmospheric sensible heat content is based on the National Centers for Environmental Protection/National Center for Atmospheric Research (NCEP/NCAR) reanalysis fields (Kalnay et al. 1996) and is shown as anomalies averaged for 1-year period. The ocean heat content curve is based on analyses of 5-year running composites of historical ocean data. Other components of atmospheric energy change, associated with changes in the latent heat of evaporation and geopotential height field, are an order of magnitude smaller than the change in sensible heat in the NCEP/NCAR analyses. The increase in observed ocean heat content is 18.2×10^{22} J (based on the linear trend for the 1957-1994 period but prorated to 1955-1996), whereas the increase in atmospheric heat content is more than an order of magnitude smaller.
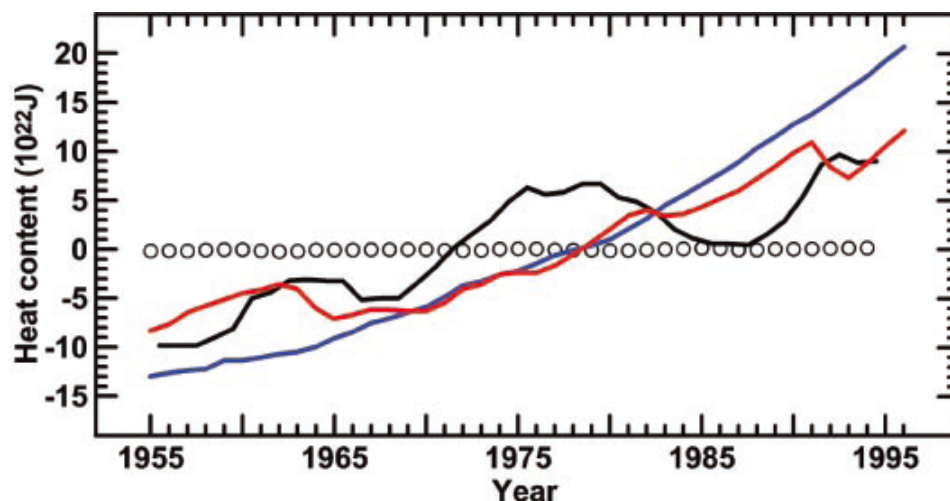
Fig. 3. Time series of various components of the observed and simulated global heat content. The observed global ocean heat content is shown in black; the open circles denote the observed global mean atmospheric heat content. The red curve denotes the ensemble mean global ocean heat content from a set of three simulations (experiment GSSV) using a coupled ocean-atmosphere model. The blue curve denotes the same for an additional set of three simulations (experiment GS), which is similar to experiment GSSV except that the radiative effects of changes in solar irradiance and volcanic aerosols are omitted.

The observed increase in oceanic heat content is compared to the simulation results of a coupled model of Earth's climate system. The coupled ocean-atmosphere-ice model is developed at the Geophysical Fluid Dynamics Laboratory (GFDL), and is higher in spatial resolution than an earlier version used in many previous studies of climate variability and change (Manabe et al. 1991; Manabe et al. 1994) but employs similar physics. The coupled model is global in domain and consists of GCMs of the atmosphere (spectral model with rhomboidal 30 truncations, corresponding to an approximate resolution of 3.75° longitude by 2.25° latitude, with 14 vertical levels) and ocean (1.875° longitude by 2.25° latitude, with 18 vertical levels). The model atmosphere and ocean communicate through fluxes of heat, water, and momentum at the air-sea interface. Flux adjustments (which did not vary interannually) are used to facilitate the simulation of a realistic mean state. Over oceanic regions, a thermodynamic sea ice model is used that includes the advection of ice by surface ocean currents.

Results are presented from two ensembles of integrations (each has three members). In the first ensemble (denoted GSSV), the radiative effects of the observed temporal variations in GHGs, sulfate aerosols, solar irradiance, and volcanic aerosols over the past century are included (Levitus et al. 2001). The ensemble members differ in their initial conditions, which are chosen from widely separated points in a 900-year-long control integration. The second ensemble (denoted GS) differs from the first by omitting the radiative effects of changes in solar irradiance and volcanic aerosols, while retaining the effects of changes in GHGs and sulfate aerosols.

For the GSSV ensemble, based on a linear trend, the simulated heat content

increased by 19.7 $\times 10^{22}$ J over the period 1955 to 1996, which is in excellent agreement

with the observed estimate (18.2 $\times 10^{22}$ J). However, it must be stressed that substantial

uncertainties exist in the specification and parameterizations of the model radiative forcing,

particularly with respect to the effects of sulfate aerosols and volcanic activity. In addition,

the ocean heat content estimates are based on a data set characterized by coverage that

varies with time (Levitus et al. 1998). Thus, the close agreement between the simulated

and observed ocean heat content increases must be evaluated in the light of these

uncertainties.

For the GS ensemble, the simulated increase of ocean heat content is approximately

70% larger than in GSSV or than the observed estimate. Based on an additional set of

experiments, the difference in ocean heat content increase between GSSV and GS is

primarily due to the radiative effects of volcanic activity. The difference between GSSV

and GS highlights the important role that volcanic activity appears to play in ocean heat

content during the late 20th century. In the GSSV ensemble, volcanoes contributed an

average global adjusted radiative forcing of -0.5W/m^2 at the tropopause over the period

1960-1999 (Andronova et al. 1999). This offsets an important fraction of the

anthropogenic forcing during the same period.

Although there is excellent agreement between the simulated and observed ocean

heat content increases over the long term (from the 1950s to the 1990s), substantial

differences exist on the decadal scale. In particular, simulated decadal variations are

smaller in amplitude than the observed variations, and there are differences in phase. The

causes of these differences need to be identified. Possible causes include an

underestimation by the model of the internal variability of the ocean-atmosphere system on decadal scales and uncertainties in the estimates of past radiative forcing. Inadequacies in the ocean observational data may also play a role.

## 4. PCM Model simulation results compared with observations

Another model is the Parallel Climate Model (PCM), which is a state-of-the-art global climate model. Using no flux-correction scheme, it is a cooperative effort between a number of universities and government laboratories in the United States.

Figure 4 shows the decadal changes over the last 45 years in the heat content of the upper 3000 m of the water column estimated from observations and a similar set of heat-content changes, relative to a 300-year control run climate, which was computed from five different realizations of the PCM forced by observed and estimated concentrations of greenhouse gases and the direct effect of sulfate aerosols in the atmosphere. There is an unexpectedly close correspondence between the observed heat-content change and the average of the same quantity from the five model realizations. These results were obtained by subsampling the model data at the same locations and times where observations existed. When the scatter between the multiple model runs is included (shaded regions), it becomes apparent that there is little or no significant difference between model and observations, even though the heat-content changes vary among ocean basins. The main exception occurs in the 1970s, when the observations show a decadal anomaly that the model runs do not reproduce. It is not possible, given the manner in which it was forced, that the model could have captured this specific decadal signal. However, the model does produce, in both its anthropogenically

forced runs and control run, decadal fluctuations that have the same magnitude and time

scale as those associated with the observed anomaly of the 1970s. In any event, the

anomaly does not alter the close correspondence between model and observations

(Barnett et al. 2001).
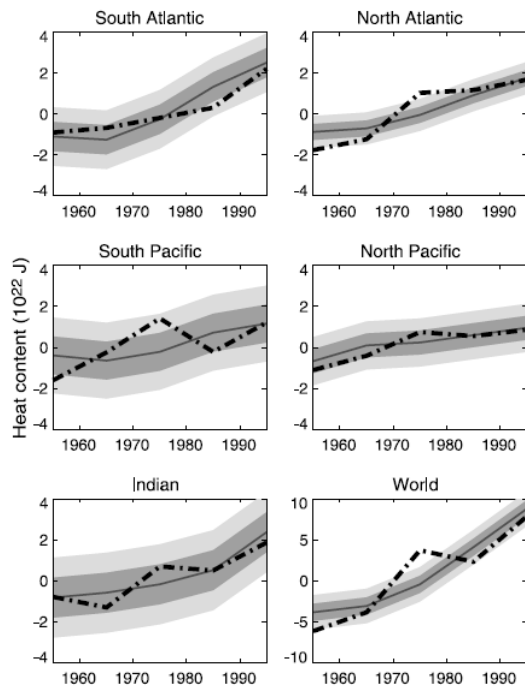
Fig. 4. Decadal values of anomalous heat content in various ocean basins. The heavy dashed line is from observations, and the solid line is the average from five realizations of the PCM forced by observed and estimated anthropogenic forcing. Both curves show significant warming in all basins since the 1950s.
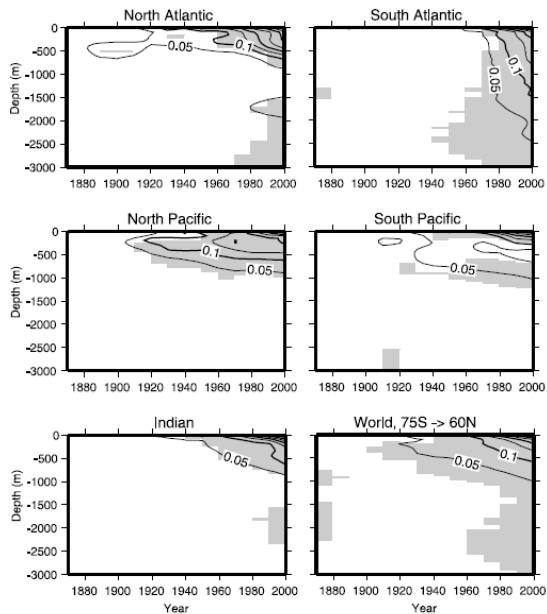
Fig. 5. Decadal temperature anomalies (°C) in various ocean basins since 1870 from the PCM. Gray-shaded regions indicate signals statistically distinguishable from zero.

The vertical development of the oceanic warming signal in the PCM for the world's

oceans is shown in Figure 5 (Barnett et al. 2001). The time evolution is from the start of

the integrations (1870) through the year 2000, for the average of the five-member

ensemble. The scatter among the five realizations allowed us to estimate a standard

deviation that was used to filter the results so that temperature anomalies exceeding a

90% confidence limit are indicated by the gray shaded areas. The nature of the warming

in the various oceans is markedly different. The Atlantic, particularly the South Atlantic,

shows strong vertical convection taking the signal to depth quite rapidly. The South

Atlantic regional average includes portions of the model's deep-water formation region in

the Weddell Sea, so the rapid penetration to depth is expected. The signal is larger in the

North Atlantic, but does not appear to penetrate as rapidly, possibly because the regional

averaging area in that ocean is large relative to the space scales of deep vertical mixing.

In the other oceans, the signal is more consistent with what one would expect from a

purely diffusive process. It is important to note that there is little deep water formed in the

South Pacific regional average, which otherwise would be expected to resemble the

South Atlantic regional average. At any rate, it is apparent that the signal in the world

ocean comes from the Atlantic in the model simulations.
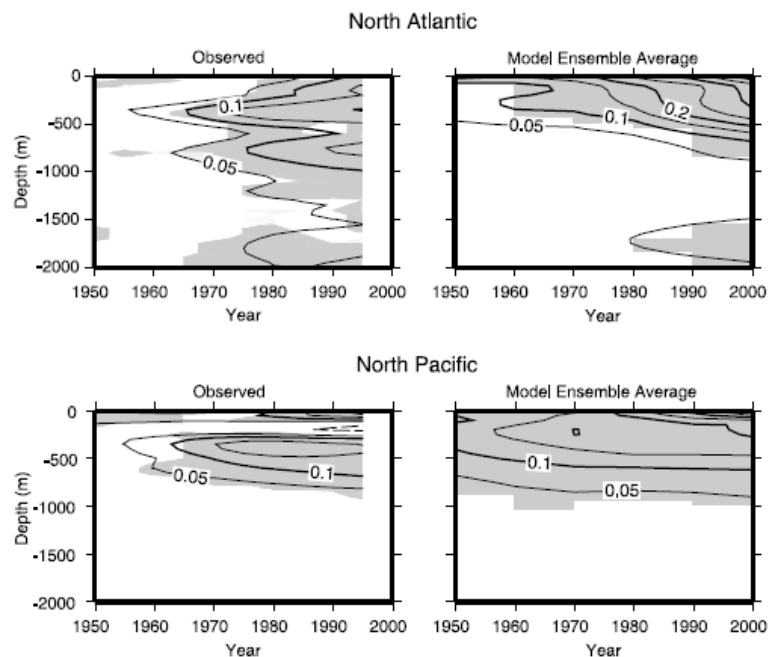
Fig. 6. . Modeled and observed temporal and vertical changes in the temperature in the
upper 2000 m of the data-rich North Pacific and North Atlantic Oceans. Grayshaded
regions denote areas where changes are statistically different from zero.

The temporal evolution of the model's vertical temperature structure is compared with

observations in Figure 6, for the North Pacific and North Atlantic Oceans. In the North

Atlantic, the observations show a near-surface warming since about 1980, whereas the

model begins warming at about 1950. This result may be partially due to the presence of a single, noisy observation set compared with the smoother, ensemble average. However, the penetration of warming with time and depth is otherwise similar between the model and observations. The more-or-less diffusive penetration in the North Pacific is captured in the model, although the very near-surface structure is again somewhat different. These discrepancies in near-surface behavior may be due to the large interannual and decadal variability that the model, running with no real-world input, cannot be expected to capture (unless it were to be forced by the observed fluxes of heat, momentum, and moisture). The model also contains no natural external forcings such as solar or volcanic mechanisms (Stott et al. 2000). The key point is that the substantial differences in the way the observed warming has penetrated to depth in the two oceans is reasonably well captured by the PCM, albeit with the caveats noted above (Barnett et al. 2001).

5. Interannual variability in upper ocean heat content

Figure 7 shows the two maps of 10-year (1993-2003) heat content change along with the data availability over the time series (Willis et al. 2004). Also shown are the zonal integrals of the maps in watts per meter of latitude. The zonal integral was used rather than the zonal average in order to reflect the contribution of each latitude band to the globally integrated rate of heat storage. It is clear that most of the signal in the 10-year change can be resolved from in situ data alone. Only in the Southern Ocean, where data are sparse, the in situ only estimate fails to recover much of the signal. The global rate of heat storage from the in situ only estimate is 0.81 W/m^2. This agrees within error bars with the 0.86 ± 0.12 W/m^2 warming rate calculated using the difference estimate. Furthermore,

the smaller in situ only warming rate is consistent with the variance reduction implied by

the altimeter twin experiment when in situ data are used to estimate a globally averaged

quantity.
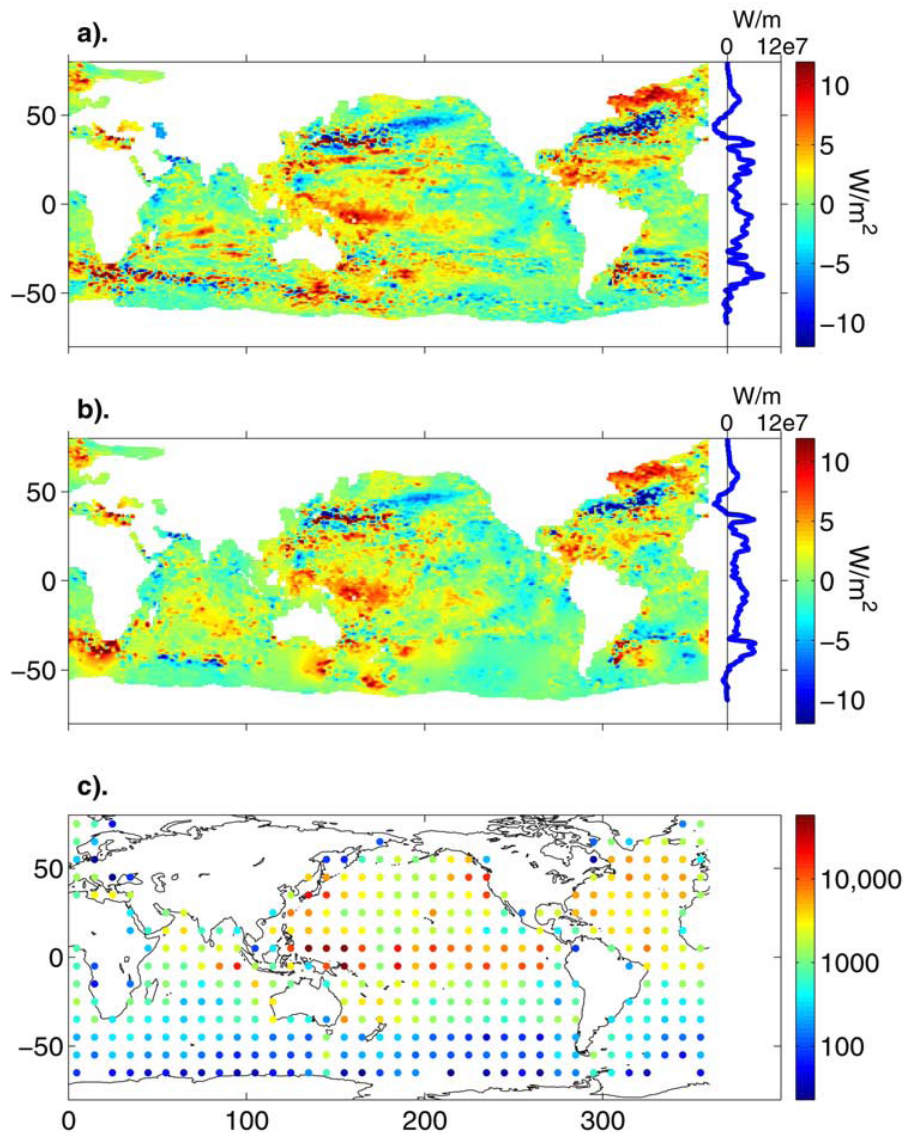
Fig. 7. Maps of 10-year change in heat content in W/m². (a) Difference estimate (combined altimeter and in situ data); (b) Estimate from in situ data alone. The curves on the right-hand side show the zonal integral of the maps in watts per meter of latitude; (c) Number of in situ profile per 10° box.

Figure 8 shows maps of heat storage calculated by differencing the heat content maps.

A large amount of interannual variability is present in the maps with the largest signals due

to the onset and decay of the 1997–1998 El Nino (Willis et al. 2004). It is evident from the

maps that interannual variability in the global average is strongly influenced by variability

in the tropics, particularly in the Pacific and Indian Oceans. Indeed, much of the interannual variability in the time series of the globally averaged heat storage is related to the El Nino Southern Oscillation (ENSO). For instance, the 1995 panel shows a substantial warming in the western tropical Pacific that marks the end of persistent El Nino conditions that lasted through the early 1990s. A similar pattern of warming is evident in 1999 and marks the onset of a persistent La Nina that remained through the latter part of the time series.
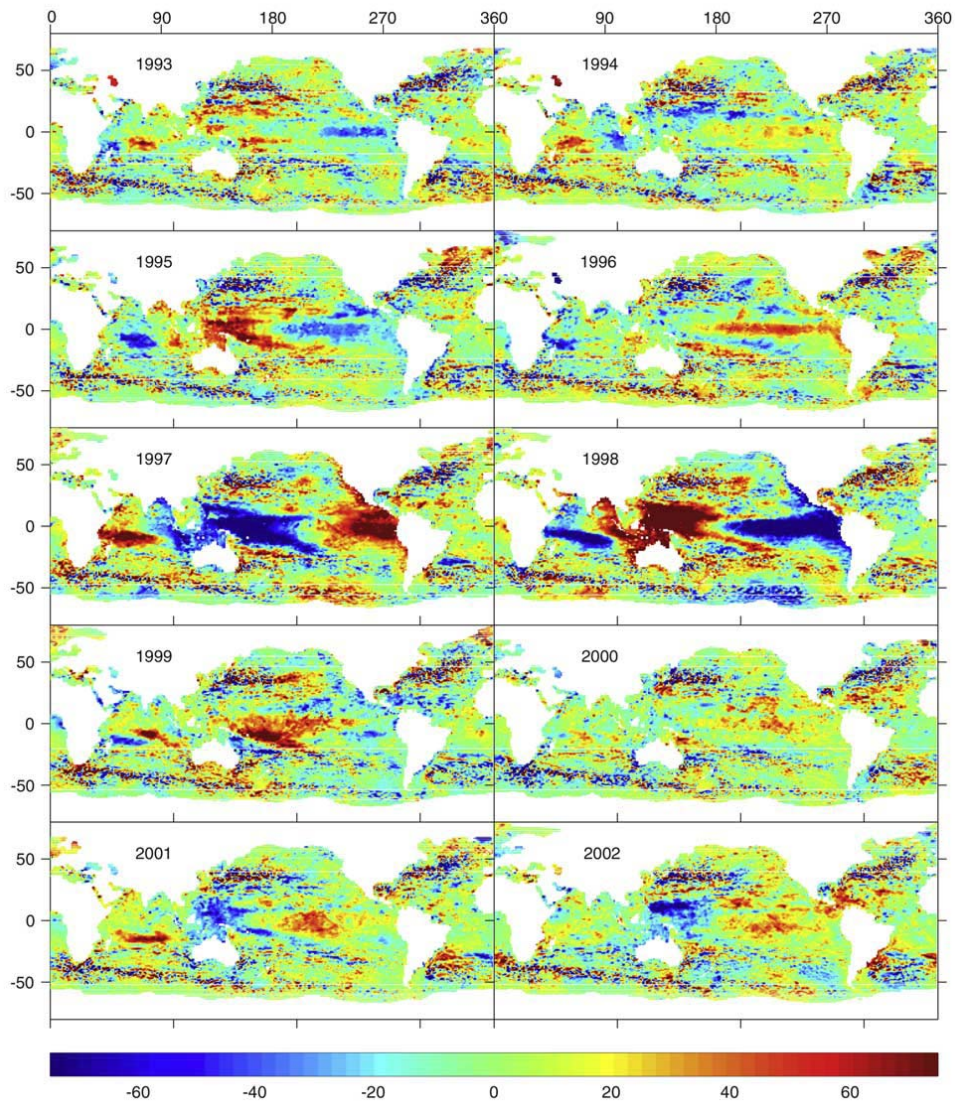

Fig. 8. Maps of heat storage variability in W/m^2. Each map is a 1-year average centered on the year shown..

In order to better illustrate the patterns of variability depicted in Figure 8, it is helpful to

compute zonal integrals over the maps of heat content. Figure 9 shows a time-latitude plot of zonally integrated heat content variability (Willis et al. 2004). Again, the most prominent feature is the 1997–1998 El Nino. Subsequent to this event, it is also possible to see the poleward propagation of a positive heat content anomaly, beginning in mid-1997 at about 20°S and continuing to 30°S by the beginning of 2000. A similar, although weaker, signal can be seen in the Northern Hemisphere at approximately the same time, suggesting that heat from the tropics propagated poleward into midlatitudes
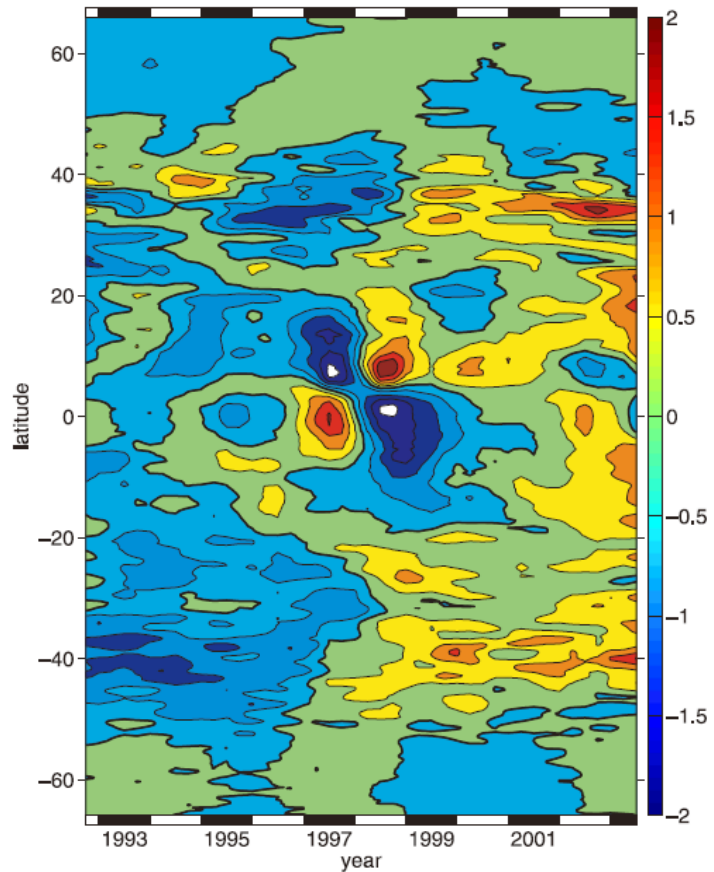
Fig. 9. Time-latitude plot of zonally integrated heat content in units of 1×10^{16} Joules per meter of latitude. Contours are 0.5×10^{16} J/m and the zero contour is thicker.
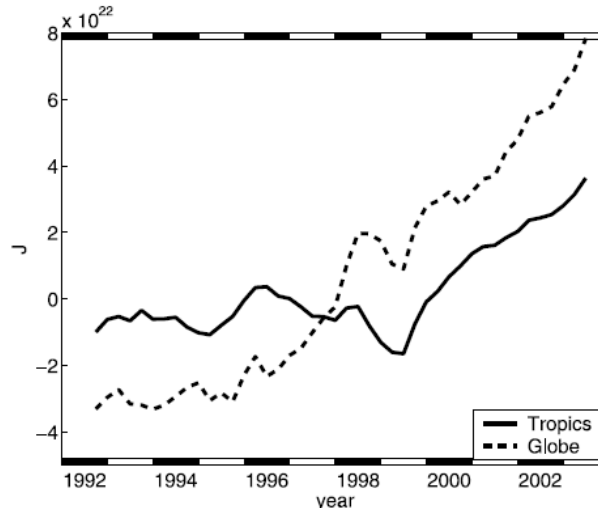
Fig. 10. Interannual variability in heat content integrated over the region from 20°N to 20°S (solid line) and over the entire globe (dashed line).

subsequent to the large 1997-1998 El Nino event. The importance of the tropical Pacific to interannual variability on global scales is further illustrated by Figure 10, which shows heat

content integrated over the region from 20°N to 20°S. The heat content in the tropics remained fairly stable through the peak of the El Nino event from late 1997 through early 1998. It then decreased rapidly through the end of 1998 and the first half of 1999. The global integral also shows heat lost during this time, but somewhat less so, suggesting that some of the heat may have been exported to the midlatitudes. The cooling, both globally and in the tropics, gives way to rapid warming in mid-1999 with the onset of La Nina. Without similar estimates of oceanic heat transport and/or surface heat flux, it is not possible to determine whether the propagation features seen in Figure 9 are the result of oceanic heat transport or are simply forced responses to signals in the atmosphere. It is clear, however, that ENSO-related variability can be large enough to affect the global oceanic heat budget on interannual timescales. In addition to ENSO, Figure 9 also shows steady warming trends in several regions. In particular, a strong, fairly linear warming trend is visible in the Southern Hemisphere, centered on 40°S. This region accounts for a large portion of the warming in the global average. Warming is also apparent at high latitudes in the Northern Hemisphere due to warming in the North Atlantic as previously documented by Levitus et al. (2000).

6. Large-scale trends in salinity for the world ocean

Figure 11 shows the linear trends representing the least-squares fit to the zonal average salinity anomaly at each latitude for each pentad from 1955-1959 through 1994-1998 for the Atlantic, Pacific, and Indian Ocean basins and the World Ocean from the surface to 3000 m depth (Boyer et al. 2005). To document the relative importance of the linear trend compared with other interannual and longer scale variability in the 44-year

record, Figure 12 shows the percent variance accounted for by the linear trend for each

basin. A significant trend is defined as an increase or decrease in salinity of more than

0.0005/yr (Boyer et al. 2005).
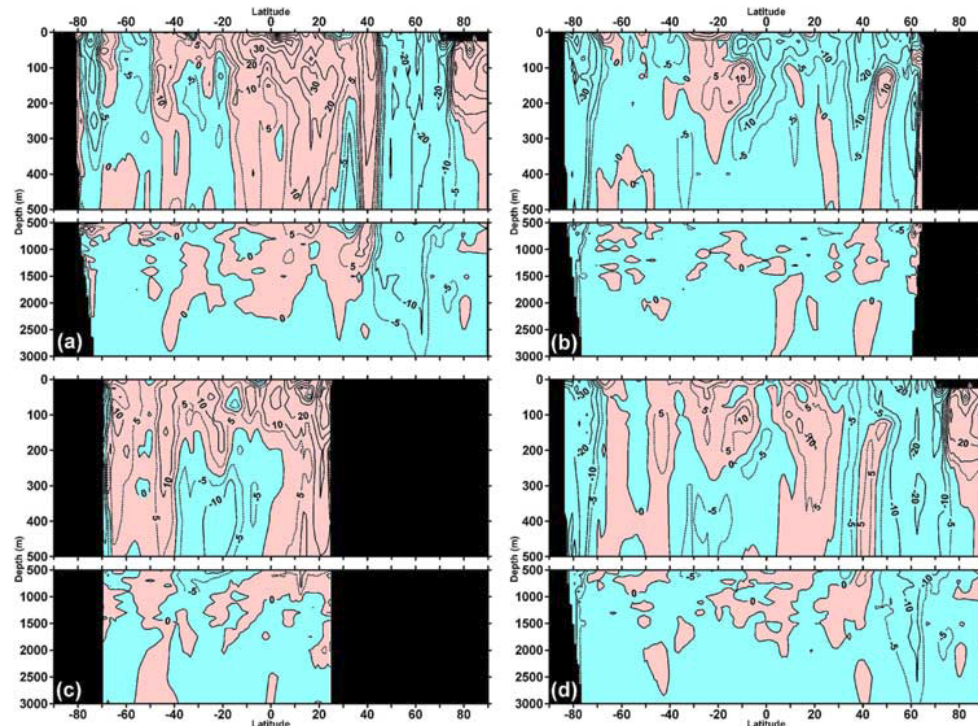
Fig. 11. Linear trend in salinity (10^{-4}/year) of the zonally averaged pentadal salinity anomaly 1955-1959
to 1994-1998 for a) Atlantic Ocean, b) Pacific Ocean, c) Indian Ocean, d) World Ocean. Negative salinity
trends are shaded blue. Positive salinity trends are shaded red.

The Atlantic Ocean exhibits a large freshening (negative salinity) trend in the subpolar

gyre from 45°N-70°N. A large positive salinity trend is present in the subtropics and tropics

in both the northern and southern hemisphere. In general, the results are characterized by

the linear trend accounting for a larger percent variance of subsurface salinity as

compared to surface variability. This reflects the fact that salinity variability is forced

entirely at the sea surface. The freshening of the subpolar gyre reaches very deep, with

values exceeding 0.0005/yr at 3000 m. The largest salinity increases occur between 20°S

and 20°N, with the changes penetrating deeper to the north of the equator. The salinity

trends in the Pacific Ocean are confined to shallower depths than in the Atlantic Ocean. Regions where the magnitude of the linear trend exceeds 0.0005/yr are confined to the top 500 m of the water column. The exception is the deep freshening south of 70°S. The one large area of increasing salinity is in the subtropic South Pacific from the sea surface down to 200 m depth. The Indian Ocean exhibits linear trends of increasing salinity at almost all latitudes from the surface down to 150 m depth. The changes are most pronounced north of 10°N. Significant salinity increase trends in this area extend to 1000 m depth. The trends in the World Ocean show changes exceeding 0.0005/yr mostly confined to the top 500 m of the water column. The exceptions are deep freshening trends in the higher latitudes of the Southern Ocean due to the Weddell and Ross Seas, and in the northern hemisphere between 50°N and 75°N due to changes in deep convection in the subpolar gyre of the North Atlantic. Both of these features reach 3000 m depth.
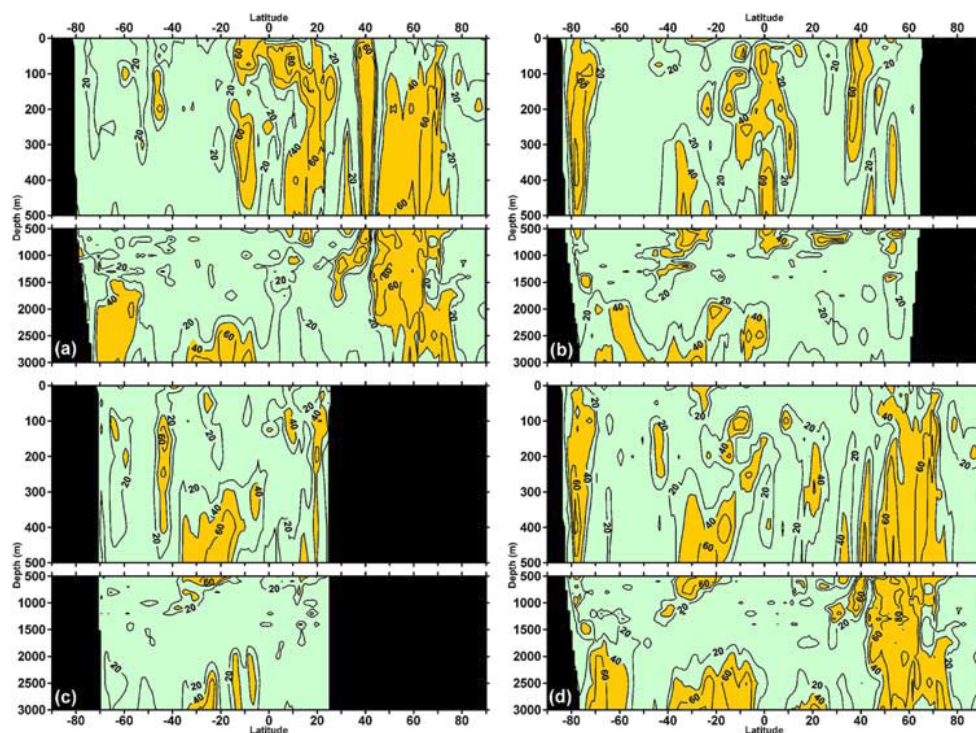
Fig. 12. Percent variance accounted for by linear trend of zonally averaged pentadal salinity anomaly 1955-1959 to 1994-1998 for a) Atlantic Ocean, b) Pacific Ocean, c) Indian Ocean, d) World Ocean. Percent variance < 60% are shaded green. Percent variance ≥ 60% are shaded orange.

7. Summary

In this review, the interannual-to-decadal variability of the heat content of the oceans from the surface through 3000 m depth during the period 1948-1998 is examined, the results of two different models forced by observed and estimated concentrations of greenhouse gases and the direct effect of sulfate aerosols on the atmosphere are compared with observations. Interannual variability in upper ocean heat content is studied using satellite altimetric height combined with in situ temperature profiles. At last, salinity changes during the period 1955-1998 for the world ocean are estimated to study the large-scale trends in salinity over this period. The agreement between model results and observational estimates of ocean heat content supports the hypothesis that increases in radiative forcing are the source of the warming observed between 1955 and 1996. Because most of the increase in radiative forcing in the latter half of the 20th century is anthropogenic, this suggests a possible human influence on observed changes in climate system heat content.

References

Andronova N. G., E. V. Rozanov, F. Yang, M. E. Schlesinger, G. L. Stenchikov, 1999: Radiative Forcing by Volcanic Aerosols from 1850 through 1994. *J. Geophys. Res.*, **104**, 16,807-16,826.

Barnett T. P., D. W. Pierce, and R. Schnur, 2001: Detection of anthropogenic climate change in the world's oceans. *Science*, **292**, 270-274.

Boyer, T. P., S. Levitus, J. I. Antonov, R. A. Locarnini, and H. E. Garcia, 2005: Linear trends in salinity for the World Ocean, 1955-1998, *Geophys. Res. Lett.*, **32**, L01604, doi:10.1029/2004GL021791.

Briffa, K. R., Jones, P. D., Schweingruber, F. H., Shiyatov, S.G. and Cook, E.R., 1995: Unusual twentieth-century summer warmth in a 1000-year temperature record from Siberia. *Nature*, **376**, 156-159.

CLIVAR, CLIVAR Science Plan, World Climate Research Programme, WCRP-89 (WMO/TD NO. 690), 1995.

Crowley, T. J., 2000: Causes of climate change over the last 1000 years, *Science*, **289**, 270–277.

Delworth, T. L., and T. R. Knutson, 2000: Simulation of early 20th century global warming. *Science*, **287**, 2246-2250.

Intergovernmental Program on Climate Change, Climate Change 1995: The Science of Climate Change, the Contribution of Working Group 1 to the Second Assessment Report of the Intergovernmental Panel on Climate Change (Cambridge Univ. Press, Cambridge, UK, 1996).

Kalnay, E., Kanamitsu, M., Kistler, R., Collins, W., 1996: The NCEP/NCAR 40-year reanalysis project. *Bull. Amer. Meteor. Soc.*, **77**, 437-471.

Levitus, S., J. Antonov, T.P. Boyer, C. Stephens, 2000: Warming of the World Ocean. *Science*, **287**, 2225-2229.

Levitus S., J. I. Antonov, J. Wang, T. L. Delworth, K. W. Dixon, and A. J. Broccoli, 2001: Anthropogenic warming of the earth's climate system. *Science*, **292**, 267–270.

Manabe, S., Stouffer, R.J., Spelman, M.J. and Bryan, K., 1991: Transient responses of a coupled ocean-atmosphere model to gradual changes of atmospheric CO2. Part I: Annual mean response. *J. Clim.*, **4**, 785-818.

Manabe, S., and R. J. Stouffer, 1994: Multi-century response of a coupled ocean-atmosphere model to an increase of atmospheric carbon dioxide, *J. Clim.*, **7**, 5-23.

Mann, M. E., R. S. Bradley, M. K. Hughes, 1998: Global-scale temperature patterns and climate forcing over the past six centuries. *Nature*, **392**, 779-787.

Mann, M. E., R. S. Bradley, and M.K. Hughes, 1999: Northern Hemisphere temperatures during the past millennium: Inferences, Uncertainties, and Limitations. *Geophysical Research Letters*, **26**, 759-762.

National Research Council, Global Environmental Change: Research Pathways for the Next Decade (National Academy Press, Washington, DC, 1999).

Nitta, T., and S. Yamada, 1989: Recent warming of tropical sea surface temperature and its relationship to the Northern Hemisphere circulation. *J. Meteor. Soc. Japan*, **67**, 375-382.

Stott, P. A. et al. 2000: External control of 20th century temperature by natural and anthropogenic forcings. *Science*, **290**, 2133–2137.

Tett, S. F. B., P. A. Stott, M. R. Allen, W. J. Ingram, and J. F. B. Mitchell, 1999: Causes of twentieth century temperature change, *Nature*, **399**, 569-572.

Trenberth K. E., in Greenhouse-Gas-Induced Climatic Change: A Critical Appraisal of Simulations and Observations, M. E. Schlesinger, Ed. (Elsevier, Amsterdam, 1991), pp. 377-390.

Willis, J. K., D. Roemmich, and B. Cornuelle, 2004: Interannual variability in upper ocean heat content, temperature, and thermosteric expansion on global scales, *J. Geophys. Res.*, **109**, C12036, doi: 10.1029/2003JC002260.